Co-published by
Institute of Fluid-Flow Machinery
Polish Academy of Sciences
Committee on Thermodynamics and Combustion
Polish Academy of Sciences

http://www.imp.gda.pl/archives-of-thermodynamics/

Effects of radiative magneto-thermal and solutal stratification on heat and mass transfer over an exponentially stretching sheet with chemical reaction

Batcha Srisailam[a], Pagilla Ramesh[b], Marla Umakanth[c], Kamatam Govardhan[d], Ganji Narender[e*]

[a]Department of Humanities and Science (Mathematics), Government Polytechnic for Women(M), Badangpet, Balapur(M), Rangareddy 500058, Telangana, India
[b]Department of Statistics and Mathematics, College of Agriculture, Professor Jayashankar Telangana Agricultural University, Hyderabad 500030, Telangana, India
[c]Department of Mathematics, CMR Engineering College, Hyderabad 501401, Telangana, India
[d]Department of Mathematics, GITAM University, Hyderabad Campus, Hyderabad 502329, Telangana, India
[e]Department of Humanities and Sciences (Mathematics), CVR College of Engineering, Hyderabad 501510, Telangana, India
*Corresponding author email: gnriimc@gmail.com

Received: 19.05.2025; revised: 20.09.2025; accepted: 08.10.2025

Abstract

A numerical investigation has been conducted on the flow of a nanofluid over an exponentially stretching surface, a configuration relevant to many industrial heat and mass transfer applications. By applying appropriate similarity transformations, the governing partial differential equations are reduced to a set of dimensionless ordinary differential equations. These nonlinear equations are solved numerically using the fourth-order Adams–Moulton method integrated with a shooting technique to ensure accuracy and stability. The validity of the computed results is established by benchmarking them against previously published findings in the literature. Key parameters influencing the flow are illustrated and discussed through graphical representations. The study's overall findings support the conclusion that increasing the Hartmann number, Schmidt number and thermal stratification parameter reduces the thermal boundary layer thickness. Moreover, enhanced solutal stratification and chemical reaction parameters are found to suppress the nanoparticle concentration. Engineering quantities like the skin friction coefficient, Nusselt number and Sherwood number are also computed and analysed, providing insights into optimising nanofluid-based thermal systems under complex boundary conditions.

Keywords: Magnetic field; Chemical reaction; Viscous dissipation; Exponential stretching sheet; Adams–Moulton method

Vol. 46(2025), No. 4, 177–186; doi: 10.24425/ather.2025.156848

Cite this manuscript as: Srisailam, B., Ramesh, P., Umakanth, M., Govardhan, K., & Narender, G. (2025). Effects of radiative magneto-thermal and solutal stratification on heat and mass transfer over an exponentially stretching sheet with chemical reaction. *Archives of Thermodynamics*, 46(4), 177−186.

1. Introduction

A nanofluid is a type of fluid that contains nanoparticles uniformly dispersed throughout a base liquid, creating a stable colloidal mixture. Typical base fluids include water, ethylene glycol and various oils, while the nanoparticles are often made of metals, metal oxides, carbides or carbon nanotubes. The term "nanofluid" was first introduced by Choi [1] to describe this novel class of fluids. Nanofluid is essentially a mixture of conventional low-thermal-conductivity fluid and nanoparticles smaller than 100 nm. It can also be defined as a suspension of tiny particles within a base fluid. The most widely used nanoparticles in nanofluids include carbon nanotubes, metals, oxides and carbides. These fluids are synthetically engineered to exhibit enhanced thermal conductivity compared to their base fluids. The thermal conductivity of nanofluids can be further improved by incorporating nanoparticles such as gold, copper and silver. Buongiorno [2] investigated the factors contributing to this enhancement and found that the increase in thermal conductivity is primarily influenced by Brownian motion and the thermophoresis effect. Nanofluids have diverse applications across various industries. In the heavy vehicle and information technol-

Nomenclature

B_0 – magnetic flux density, T
C – concentration, kg/m^3
C_f – skin friction coefficient
D – diffusion coefficient, m^2/s
Ec – Eckert number
M – Hartmann number
Nb – Brownian motion parameter
Nt – thermophoresis parameter
Nu – Nusselt number
P – pressure, Pa
Pr – Prandtl number
R – thermal radiation parameter
Sc – Schmidt number
Sh – Sherwood number
Sm – thermal solutal stratification parameter
St – thermal stratification parameter
T – temperature of the fluid, K
u – velocity in x-direction, m/s
v – velocity in y-direction, m/s
x, y – Cartesian coordinates, m

Greek symbols

α – thermal diffusivity, m^2/s
γ – chemical reaction parameter
θ – dimensionless temperature
κ – thermal conductivity, W/(m K)
λ_r – porosity parameter
μ – fluid dynamic viscosity, Pa s
ν – kinematic viscosity, m^2/s
ρ – fluid density, kg/m^3
σ – electrical conductivity, S/m
ϕ – nanoparticle volume fraction

Abbreviations and Acronyms

KVL – Khanafer-Vafai-Lightstone (model)
MHD – magnetohydrodynamics
ODEs – ordinary differential equations
OHAM – optimal homotopy asymptotic method
PDEs – partial differential equations

ogy sectors, they are used as coolants to improve heat dissipation. Additionally, nanofluids play a crucial role in industrial, biomedical and technological fields, making them a valuable innovation.

Other characteristics of the nanofluids, such as volume concentration, particle agglomeration, thermophoresis, Brownian motion, surface area, particle shape, etc., should be considered for the nanofluids to perform more effectively due to their numerous remarkable uses in a variety of industrial and scientific fields, including the production of rubber and plastic sheets, geothermal energy extraction, fiber glass, hot rolling, etc. The fluid dynamics community has given the study of boundary layer nanofluid flow a great deal of attention. To investigate the rotating flow of nanofluids induced by an exponentially stretched layer, Mushtaq et al. [3] carried out a numerical analysis.

The word magnetohydrodynamics originates from magneto, meaning magnetic field; hydro, referring to fluid; and dynamics, which denotes motion. These three concepts are combined to form the term magnetohydrodynamics (MHD). The magnetic characteristics of an electrically conducting fluid are examined via hydromagnetic flow. When a conducting fluid moves through a magnetic field, it generates an electric current, leading to the formation of the Lorentz force, which alters the fluid's motion. The MHD effect plays a crucial role in regulating cooling rates and achieving desired material properties. Shit et al. [4] analysed unsteady MHD nanofluid flow and heat transfer over an exponentially stretching surface with radiation and porous medium effects. Numerical results show that Brownian motion, thermophoresis and magnetic field enhance thermal boundary layers, while unsteadiness reduces them. Entropy generation is strongly influenced by magnetic field, dissipation, radiation and Biot number.

Reddy and Chamkha [5] examined the MHD nanofluid flow of Al_2O_3–water and TiO_2–water past a stretching sheet within a porous medium, accounting for radiation, chemical reaction and heat source/sink effects. Their work employed a validated finite element approach to solve the governing equations and assessed the impact of critical parameters on velocity, temperature and concentration distributions.

Additionally, Gupta et al. [6] analysed MHD stagnation point flow of a non-Newtonian nanofluid past an inclined stretching sheet, incorporating chemical reaction, thermal radiation, Brownian motion and thermophoresis. By applying the optimal homotopy asymptotic method (OHAM), they examined the influence of various parameters on flow and heat transfer, confirming the method's superiority over conventional techniques. More recently, Gireesha et al. [7] studied unsteady nanofluid flow with dust particles over a stretching sheet under Hall current effects. Using the Khanafer-Vafai-Lightstone (KVL) model and similarity transformations, they reported that dust suspension and Hall current significantly enhance heat transfer and the Nusselt number.

For a continuous surface that is stretching exponentially, Magyari and Keller [8] outlined the features of mass and transmission of heat in the boundary layer. Other pertinent research studies were conducted by Vajravelu [9]. Cortell [10] studied how viscous dissipation via a nonlinear stretching affected the thermal boundary layer. Narender et al. [11] contemplated the radiation effects in the presence of heat generation/absorption and magnetic field on the magnetohydrodynamics (MHD) stagnation point flow over a radially stretching sheet using a Casson nanofluid. Narender et al. [12] explored the impacts of external magnetic field inclinations and viscous dissipation due to heat generation or absorption parameter on MHD mixed convective flow of Casson nanofluid. Murugesan and Kumar [13] also elucidated the same effect but with the flow of nanofluid over the exponentially stretching sheet. Hayat and Nadeem [14] examined hybrid nanofluids in a 3D rotating stretching sheet with radiation, heat generation and chemical reaction, showing that they achieve higher heat transfer rates than conventional nanofluids. This topic was then continued by Hayat et al. [15], who investigated the influence of MHD, heat generation/absorp-

tion and nanoparticle concentration on hybrid nanofluid flow over a rotating stretching surface. They analysed the effects on velocity, skin friction and heat transfer, showing that hybrid nanofluids outperform conventional nanofluids. Other researchers [16–19] have studied boundary layer flow over a stretching sheet, where the velocity increases linearly from a fixed point.

Chemical reactions are crucial components in numerous living and non-living processes. Examples of their applications include burning fuels, the production of glass and pottery, iron smelting and food processing. Chemical reactions are categorised as homogeneous and heterogeneous, with the rate at which they occur depending on the concentration of the participating reactants. At the heart of chemical engineering, chemical reactions are employed to produce high-quality substances from natural raw materials. It is crucial to streamline a reaction, thereby optimising its quality and yield while minimising the use of reactants, energy and hazardous by-products. Researchers, engineers and academicians are increasingly showing a keen interest in developing efficient and sustainable chemical reaction systems. Researchers led by Swapna examined the flow of a magneto-micropolar nanofluid above a heated, permeable sheet that stretches, incorporating nonlinear radiation, chemical reaction and viscous dissipation effects [20]. Researchers led by Reddy et al. [21] investigated the influence of an inclined magnetic parameter on the unsteady, two-dimensional flow of an incompressible, viscous fluid confined between parallel plates.

The field of heat generation/absorption is a collaborative effort, essential in managing the heat transfer performance. This has led to numerous investigations into the effects of heat generation/absorption on nanofluids. These studies have consistently shown that increased heat generation leads to a rise in the temperature profile. Notably, Thirupathi et al. [22] conducted a comprehensive study on a nonlinear stretching sheet, examining thermal radiation, viscous dissipation, heat source and chemical reaction in Casson nanofluid flow. Eid and Nafe [23] showed that Fe_3O_4–Cu/EG (ethylene glycol) hybrid nanofluid enhances heat transfer over shrinking/stretching sheets, with effects influenced by nanoparticle concentration, flow type and MHD conditions. The relevant literature for these studies can be found in [24−26].

Our study examines nanofluid flow over an exponentially stretching sheet, with particular attention to the effect of chemical reaction. Since these conditions have not been studied together in prior research Hayat et al. [27], we aim to analyse the flow behaviour under this unique configuration. The series expressions for velocity, temperature and nanoparticle concentration are developed by the method of Adams-Moulton of fourth order with a shooting technique. The numerical solutions are obtained by the software FORTRAN Language program. The organisation of this article is structured as: Section 2 outlines the problem formulation and the essential physical quantities of interest. Section 3 describes the application of the Adams-Moulton method to the proposed problem. Section 4 reviews the results, whereas Section 5 is reserved for concluding observations.

1.1. Core objectives of the thermal transport analysis

The core objectives are:

- To model the flow and heat transfer characteristics of a nanofluid over an exponentially stretching sheet, incorporating magnetic field effects, chemical reactions and heat generation or absorption.
- Also, explore how significant physical parameters influence the velocity, temperature and concentration profiles within the boundary layer.
- Utilise the Adams–Moulton method with a shooting technique for solving the governing equations.
- Analyse critical engineering indicators, such as local skin friction and Nusselt number, to evaluate heat transfer performance and surface resistance.
- Consider the practical insights into improving thermal performance in engineering applications by evaluating the combined impact of magnetic, thermal and chemical effects on nanofluid behaviour.

1.2. Novel contributions and significance of the study

- To our knowledge, this study offers the framework of nanofluid flow over a stretching sheet in which chemical reaction and radiative heat transfer are included.
- The incorporation of chemical reactions into the model adds greater physical fidelity and enhances its applicability to real-world thermal systems where reactive processes are significant.
- This work obtains coupled ODEs from highly nonlinear governing PDEs through similar transformations and, consequently, makes numerical analyses easier to perform.
- The study is applicable to advanced technologies such as electronic cooling systems, biomedical applications, waste heat recovery and environmental systems.

2. Problem statement and mathematical formulation

Let us consider the steady fully developed incompressible nanofluid flow along a continuously exponentially stretching sheet subject to a transverse magnetic field of strength B_0 in the presence of thermal radiation and chemical reaction.

The x-axis is aligned with the sheet length, while the y-axis is normal to it. The stretching sheet velocity is $u_w = U_0 \cdot e^{x/L}$. The flow is confined to $y > 0$. Figure 1 illustrates the schematic of our study.

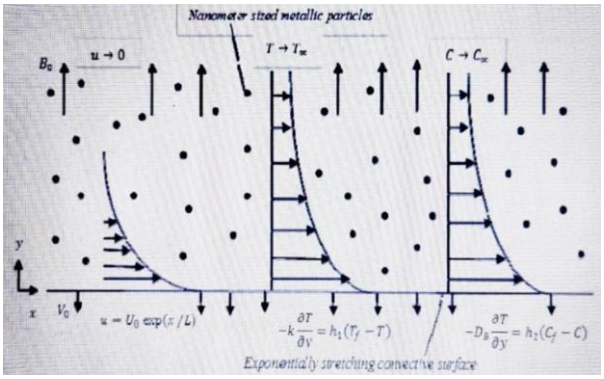

Fig. 1. Configuration of the flow.

The temperature and concentration at the wall and away from it are regarded to be exponentially stratified $T_w = T_0 + be^{x/2L}$, $C_w = C_0 + ae^{x/2L}$, $T_\infty = T_0 + ce^{x/2L}$, $C_\infty = C_0 + de^{x/2L}$, respectively ($a$, b, c and d constants).

The considered formulations for this system, expressed using the equations of continuity, momentum, energy and nanoparticle concentration, are as follows [17,27]:

$$\frac{\partial u}{\partial x} + \frac{\partial v}{\partial y} = 0, \tag{1}$$

$$\rho\left(u\frac{\partial u}{\partial x} + v\frac{\partial u}{\partial y}\right) = \mu\frac{\partial^2 u}{\partial y^2} - \frac{\mu}{K}u - \sigma B_0^2 u, \tag{2}$$

$$\left.\begin{aligned} u\frac{\partial T}{\partial x} + v\frac{\partial T}{\partial y} = \frac{k}{(\rho C_p)_f}\left(\frac{\partial^2 T}{\partial x^2} + \frac{\partial^2 T}{\partial y^2}\right) + \\ + \frac{(\rho C_p)_p}{(\rho C_p)_f}\left[D_B\frac{\partial C}{\partial y}\frac{\partial T}{\partial y} + \frac{D_T}{T_\infty}\left(\frac{\partial T}{\partial y}\right)^2\right] + \\ + \frac{16\sigma^* T_\infty^3}{k^*(\rho C_p)_f}\frac{\partial^2 T}{\partial y^2} + \frac{\mu}{(\rho C_p)_f}\left(\frac{\partial u}{\partial y}\right)^2, \end{aligned}\right\} \tag{3}$$

$$u\frac{\partial C}{\partial x} + v\frac{\partial C}{\partial y} = D_B\left(\frac{\partial^2 C}{\partial x^2} + \frac{\partial^2 C}{\partial y^2}\right) + \frac{D_T}{T_\infty}\frac{\partial^2 T}{\partial y^2} - K_1(C - C_\infty), \tag{4}$$

along with:

$y = 0$:

$$\left.\begin{aligned} u = u_w = U_0 e^{\frac{x}{L}}, \\ v = 0, \\ T = T_w = T_0 + be^{\frac{x}{2L}}, \\ C = C_w = C_0 + ae^{\frac{x}{2L}}, \end{aligned}\right\} \tag{5a}$$

$y \to \infty$:

$$\left.\begin{aligned} u \to 0, \\ v \to 0, \\ T = T_\infty = T_0 + ce^{\frac{x}{2L}}, \\ C = C_\infty = C_0 + de^{\frac{x}{2L}}. \end{aligned}\right\} \tag{5b}$$

Equations (1) to (4) show how mass, momentum and energy are conserved in the system and include the equation for how concentration changes. In these equations, u and v are flow speeds in the x and y directions; T is temperature; ϕ - nanoparticle volume fraction; density is denoted by ρ; electrical conductivity by σ; the kinematic viscosity by ν; μ - dynamic viscosity; K - porous medium permeability; $(C_p)_f$ - fluid heat capacity; $(C_p)_p$ - nanoparticle heat capacity; D_B - Brownian diffusion coefficient; D_T - thermophoresis coefficient; and T_∞ - ambient temperature.

The radiative heat flux vector can be described as:

$$q_r = \frac{-4\sigma^*}{3k^*}\frac{\partial T^4}{\partial y}, \tag{6}$$

where σ^* and k^* denote the Stefan-Boltzmann constant and the mean absorption coefficient, respectively, and is linearised via a Taylor series expansion about T_∞, from which we get:

$$\Rightarrow \frac{\partial T^4}{\partial y} = 4T_\infty^3\frac{\partial T}{\partial y}. \tag{7}$$

Using Eq. (7) in Eq. (6) and differentiating, we have the following form:

$$\frac{\partial q_r}{\partial y} = -\frac{16\sigma^* T_\infty^3}{3k^*}\frac{\partial^2 T}{\partial y^2}. \tag{8}$$

To find the solution of our model, we use the following similarity transformation [13,27]:

$$\left.\begin{aligned} \eta = y\sqrt{\frac{U_0}{2\nu_f L}}e^{\frac{x}{2L}}, \\ v = -\sqrt{\frac{\nu_f U_0}{2L}}e^{\frac{x}{2L}}[f(\eta) + \eta f'(\eta)], \\ u = U_0 e^{\frac{x}{2L}}f'(\eta), \\ \theta(\eta) = \frac{T - T_\infty}{T_w - T_0}, \quad \phi(\eta) = \frac{C - C_\infty}{C_w - C_0}. \end{aligned}\right\} \tag{9}$$

Using Eq. (9), the governing equations (2-4) transform to new equations:

$$f''' - (M + \lambda)f' - 2(f')^2 + ff'' = 0, \tag{10}$$

$$\left.\begin{aligned} \frac{\left(1+\frac{4R}{3}\right)}{\Pr}\theta'' + Nb\theta'\phi' + Nt(\theta')^2 + \mathrm{Ec} + \\ -f'(St + \theta) + \theta' f = 0, \end{aligned}\right\}, \tag{11}$$

$$\phi'' + \frac{Nt}{Nb}\theta'' + \mathrm{Sc}(f\phi' - f'\phi) - \mathrm{Sc}(Smf' - \gamma\phi) = 0, \tag{12}$$

together with:

$$\begin{aligned} f'(0) = 1, \quad f(0) = 0, \quad f'(\infty) = 0, \\ \theta(0) = 1 - Sm, \quad \theta(\infty) = 0, \\ \phi(0) = 1 - St, \quad \phi(\infty) = 0. \end{aligned} \tag{13}$$

Different parameters used in the ordinary differential equations (ODEs) (10–12) and boundary conditions (13) have been listed in Table 1.

The local skin friction, Nusselt number and Sherwood number can be defined:

$$C_f = \left[\frac{\tau_w}{\left(\frac{1}{2}\right)\rho U_0^2 e^{\frac{2x}{L}}}\right]_{y=0},$$

$$\mathrm{Nu} = \frac{-xq_w}{k(T_w - T_\infty)},$$

$$\mathrm{Sh} = \frac{-xq_m}{D_B(C_w - C_\infty)},$$

$$\left.\begin{aligned} C_f\sqrt{\frac{\mathrm{Re}_x}{2}} = f''(0), \\ \mathrm{Nu}\mathrm{Re}_x^{-1/2}\sqrt{\frac{2L}{x}} = -\frac{1}{1-St}\theta'(0), \\ \mathrm{Sh}\mathrm{Re}_x^{-1/2}\sqrt{\frac{2L}{x}} = -\frac{1}{1-Sm}\phi'(0), \end{aligned}\right\} \tag{14}$$

where $\mathrm{Re}_x = U_0 e^{\frac{x}{l}}\frac{x}{\nu}$ is the local Reynolds number.

Table 1. Various dimensionless parameters utilised in the governing ODEs and their typical ranges of variation.

Model parameter	Definition	Significance	Typical ranges used
Porosity parameter (λ)	$\frac{\nu_f L}{KU_0} e^{-\frac{x}{L}}$	Impact on the material's ability to store and transport fluids	0.2 to 0.7. For example, sandstones typically have a porosity of 10–40% (0.1–0.4), while peats can exceed that of 50% (0.5).
Hartmann number (M)	$\frac{2\sigma B_0^2(x)L}{\rho_f U_0}$	The ratio of Lorentz force to viscous force in the fluid.	0 to 100, often in the range of 0.1 to 10 for many theoretical studies on MHD flows.
Prandtl number (Pr)	$\frac{\nu_f(\rho C_p)_f}{k_f}$	Momentum to thermal diffusivity	A Prandtl number of Pr = 1.7 corresponds to water at relatively high temperatures, such as near its boiling point
Thermal radiation parameter (R)	$\frac{4\sigma^* T_\infty^3}{k_0 k}$	Ratio of radiative heat flux to conductive heat transfer.	Often investigated in the range of 0.1 to 10, with higher values signifying more dominant radiation effects, common in high-temperature processes like those in furnaces or solar collectors.
Viscous parameter (Eckert number) (Ec)	$\frac{{U_0}^2 e^{\frac{x}{2L}}}{(c_p)(T_f - T_\infty)}$	The relationship between a flow's kinetic energy and the boundary layer enthalpy difference.	Values can vary widely depending on the flow speed, from very small (Ec<<1) for low-speed flows to values near 1.0 for high-speed flows where viscous heating becomes significant.
Thermal stratification parameter (St)	$\frac{c}{b}$	Buoyancy forces to mixing forces in a fluid system	The effect is significant in situations where the temperature varies, with values ranging from 0.0 to 1.0 or more, with 0.0 indicating no stratification.
Thermal solutal stratification parameter (Sm)	$\frac{d}{a}$	Ratio of thermal buoyancy forces to solutal buoyancy forces	Similar to thermal stratification, it is typically investigated in the range of 0.0 to 1.0 or more, with 0.0 representing a uniform concentration
Brownian motion parameter (Nb)	$\frac{\tau D_B(C_w - C_\infty)}{\nu}$	The effect of random thermal fluctuations on the diffusion of nanoparticles in a fluid.	Typically studied within the range of 0.1 to 1.0, though some studies use values up to 5.0 to explore pronounced effects.
Thermophoresis parameter (Nt)	$\frac{\tau D_T(T_w - T_0)}{\nu(T_\infty)}$,	The ratio of thermophoretic forces to viscous forces.	Generally considered in the range of 0.1 to 1.0 in most nanofluid studies.
Schmidt number (Sc)	$\frac{\nu}{D_B}$	The ratio of momentum diffusivity (viscosity) to mass diffusivity	For gases, it's typically close to 1.0 (around 0.2 to 4.0). For liquids, values are much higher, ranging from 200 to 1500, indicating that momentum diffuses much faster than mass.
Chemical reaction parameter (γ)	$\frac{K_0 L}{U}$	Ratio of reaction rate to transport rate (diffusion or convection)	Ranges from small values (approaching 0 for slow reactions) to higher values (e.g., 1.0 to 5.0) for moderate to fast reactions.

3. Implementation of the numerical scheme

The ODEs (10–12) along with boundary conditions (BCs) stated in (13) have been explored numerically via a shooting technique. After performing successive iterations, the bounded domain $[0, \eta_{\max}]$ has been considered instead of $[0, \infty]$ for an appropriate value of $\eta_{\max}$, the value after which the solution converges asymptotically. The variable f is denoted by y_1, θ by y_4 and ϕ by y_6. The boundary value problem (BVP) (10)–(13) in new variables is converted into an initial value problem (IVP):

$$\left.\begin{aligned}
y_1' &= y_2, & y_1(0) &= 0,\\
y_2' &= y_3, & y_2(0) &= 1,\\
y_3' &= [2y_2^2 - y_1 y_3 + (M+\lambda)y_2], & y_3(0) &= s,\\
y_4' &= y_5, & y_4(0) &= 1 - Sm,\\
y_5' &= -\frac{3\mathrm{Pr}}{(3+4R)}\begin{bmatrix} y_1 y_5 + Nb\, y_5 y_7 + Nt\, y_7^2 + \\ +\mathrm{Ec}(f'')^2 - y_2(St + y_4) \end{bmatrix}, & y_5(0) &= t,\\
y_6' &= y_7, & y_6(0) &= 1 - St,\\
y_7' &= \frac{Nt}{Nb} y_5' - Sc(y_1 y_7 - y_2 y_6) + ScSm y_2 + Sc\gamma y_7, & y_7(0) &= u\,.
\end{aligned}\right\} \quad (15)$$

The above equations are solved using the shooting technique along with the Adams-Moulton method of order 4 with an initial guess s, t and u. The missing initial conditions s, t, u are chosen such that:

$$y_2(\eta, s, t, u) = 0, \quad y_4(\eta, s, t, u) = 0, \quad y_6(\eta, s, t, u) = 0. \quad (16)$$

To solve the system of algebraic equations (16), we use Newton's method. The iterative process is repeated until the following criteria is met:

$$\max\{|y_2(\eta_{\max}) - 0|, |y_4(\eta_{\max}) - 0|, |y_6(\eta_{\max}) - 0|\} < \xi.$$

Throughout this work, ξ has been taken as 10^{-7} unless otherwise mentioned.

4. Analysis of results and validation

To clearly provide physical insight into the heat and mass transfer of an MHD nanofluid in the presence of viscous dissipation, thermal radiation parameter, hear generation/absorption and chemical reaction. In this complex geometry, we focused on the impact of the Hartmann number, the porosity parameter ($0 \le M, \lambda \le 1$), the Brownian motion parameter ($1.0 \le Nb \le 1.6$), the thermophores parameter ($0.1 \le Nt \le 0.6$), thermal stratification parameter ($0.1 \le St \le 0.4$), thermal radiation parameter

($0.1 \le R \le 0.4$), Eckert number ($0 \le \mathrm{Ec} \le 1.1$), the Schmidt number ($0.9 \le \mathrm{Sc} \le 1.3$), the solutal stratification parameter ($0.1 \le Sm \le 0.8$) and the chemical reaction parameter ($0.1 \le \gamma \le 0.4$) on the flow structures, velocity, temperature and concentration of the nanoparticles. For validation, the results of this study show the Schmidt number compared with previously published findings by Hayat et al. [27]. The numerical values of $-f''(0)$ are computed and compared in Table 2 for the case of $M = \lambda = 0$. We observe that the present and previous results are found to be in reasonable correlation. Thus, we guarantee that the technique, as well as the results provided in this present study, are valid and acceptable. Table 3 provides numerical results for the Nusselt number and Sherwood number for different flow impact factors. As anticipated, the Nusselt number reduces as the Schmidt number (Sc), the solutal stratification parameter (Sm) and chemical reaction parameter (γ) rise, while the opposite phenomenon is identified for the Sherwood number.

Table 2. The comparison between the previous and present results of $-f''(0)$ for $M = \lambda = 0$.

Value of	Hayat et al. [27]	Present
$-f''(0)$	1.281808	1.2818170
$f(\infty)$	0.905639	0.9050169

Table 3. Nusselt number and Sherwood number for $M = 0.1$, $\lambda = 0.1$, Ec = 0.5, Pr = 1.7, $Nt = Nb = 0.8$, $R = 0.4$ and different values of Sc, St, Sm, γ.

Sc	St	Sm	γ	$-\theta'(0)$	$-\frac{\theta'(0)}{(1-St)}$	$-\phi'(0)$	$-\frac{\phi'(0)}{(1-St)}$
1.1				0.3952224	0.4391360	0.7880001	0.8755557
1.2	0.1	0.1	0.1	0.3885755	0.4317505	0.8556961	0.9507734
1.5				0.3719586	0.4132873	1.042329	1.1581430
	0.2			0.4570068	0.5712585	0.6412907	0.7125453
1.1	0.3	0.1	0.1	0.5208401	0.7440573	0.4927663	0.5475181
	0.5			0.6548117	1.3096230	0.1901195	0.2112439
		0.2		0.3322426	0.3691584	0.8856008	1.1070010
1.1	0.1	0.3	0.1	0.2690218	0.2989132	0.9830891	1.4044130
		0.5		0.1417351	0.1574834	1.1778130	2.3556250
				0.2936075	0.3262306	0.8585148	0.9539053
1.1	0.1	0.1	0.1	0.2507791	0.2786434	0.8873966	0.9859962
				0.1275781	0.1417534	0.9683428	1.0759360
			0.2	0.2398219	0.2664688	1.0439920	1.1599910
1.1	0.1	0.1	0.3	0.2360424	0.2622693	1.1074420	1.2304910
			0.5	0.2302854	0.25587260	1.2173230	1.3525810

Figure 2 illustrates the impact of the Hartmann number (M) on the velocity field f'.

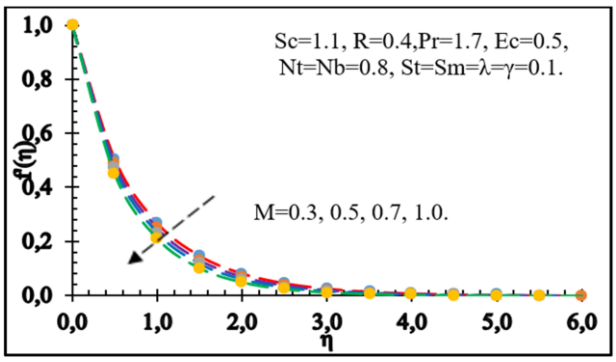

Fig. 2. Variation in $f'(\eta)$ with M.

As M increases, a noticeable decrease in the velocity profile is observed. This reduction occurs because the presence of a magnetic field generates a resistive force known as the Lorentz force. The Lorentz force acts as a damping mechanism by opposing the motion of the fluid, thereby reducing its velocity. Physically, this force arises due to the interaction between the induced electric currents within the fluid and the applied magnetic field, leading to an increase in the resistive effect. Consequently, as M increases, the influence of the Lorentz force becomes more significant, further suppressing the fluid's motion and causing a more pronounced decline in the velocity profile.

Figure 3 presents the temperature field for varying values of the Brownian motion parameter (Nb) and the thermophoresis parameter (Nt).

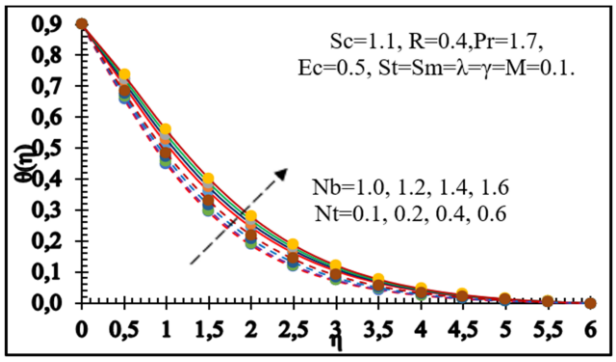

Fig. 3. Variation in $\theta(\eta)$ with Nb and Nt.

The figure reveals that as the values of Nb and Nt increase, both the temperature profile and the thermal boundary layer thickness exhibit significant enhancement. This increase occurs because Brownian motion, which describes the random movement of nanoparticles in the fluid, contributes to increased ther-

mal energy transport, thereby raising the temperature distribution. Similarly, thermophoresis, which refers to the movement of particles due to temperature gradients, leads to the migration of nanoparticles from hotter to cooler regions, further influencing heat transfer. As a result, the combined effect of higher *Nb* and *Nt* leads to a more pronounced thermal boundary layer, indicating an overall rise in the temperature profile throughout the flow region.

Figure 4 illustrates the concentration profile for different values of *Nb* and *Nt*.

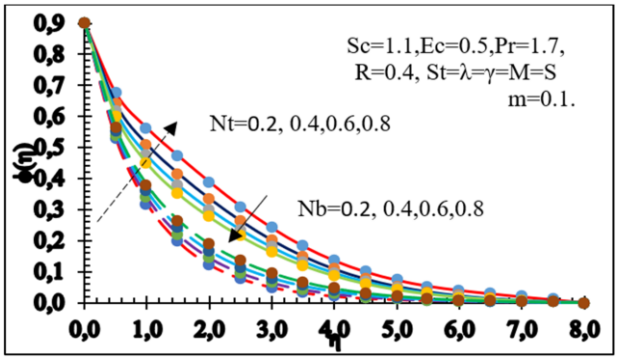

Fig. 4. Variation in $\phi(\eta)$ with *Nb* and *Nt*.

As the Brownian motion parameter (*Nb*) increases, the random movement of particles intensifies, enhancing diffusion and promoting a more uniform distribution. This increased dispersion reduces localised particle accumulation, leading to a lower overall concentration. Conversely, a higher thermophoresis parameter (*Nt*) results in greater particle accumulation in cooler regions. Thermophoresis drives particles away from hotter areas due to temperature-induced force imbalances, causing them to concentrate in lower-temperature zones. Unlike Brownian motion, which enhances mixing, thermophoresis induces directional transport, leading to localised clustering. The balance between these effects governs the overall particle distribution in the fluid.

Figure 5 illustrates the effect of the thermal stratification parameter (*St*) on temperature, showing that as *St* increases, the overall temperature decreases and the temperature difference between the surface and the surrounding fluid diminishes.

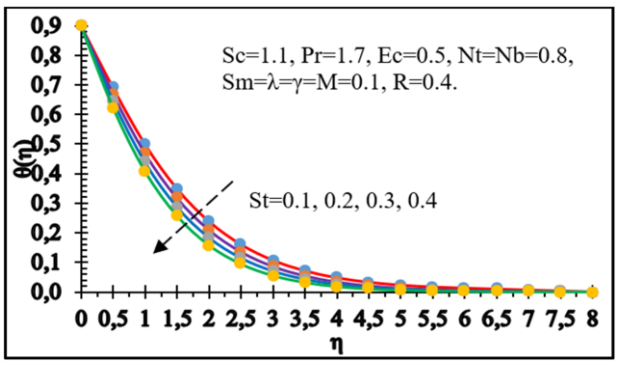

Fig. 5. Variation in $\theta(\eta)$ with *St*.

Physically, a higher *St* represents stronger thermal stratification, which enhances heat dissipation and restricts heat retention near the surface. This leads to a more uniform temperature distribution, reducing thermal gradients and limiting heat transfer between layers.

As observed in Fig. 6, the dimensionless temperature increases with a higher radiation parameter (*R*). Physically, this occurs because an increase in R corresponds to a decrease in the mean absorption coefficient (k^*), which reduces the fluid's ability to absorb radiation. However, at the same time, the overall rate of radiative heat transfer to the fluid increases, thereby supplying additional thermal energy and raising the fluid temperature. The enhanced radiative heat transfer leads to a more uniform temperature distribution and thicker thermal boundary layer, reducing temperature gradients and slowing heat dissipation.

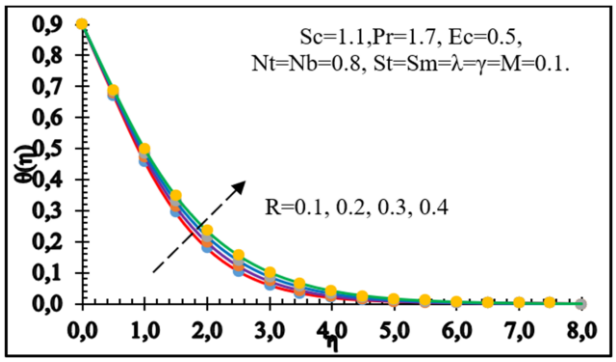

Fig. 6. Variation in $\theta(\eta)$ with *R*.

The fluid viscosity is highly sensitive to temperature changes, and as shown in Fig. 7, the temperature increases with the increasing Eckert number (Ec) due to the effect of resistive forces.

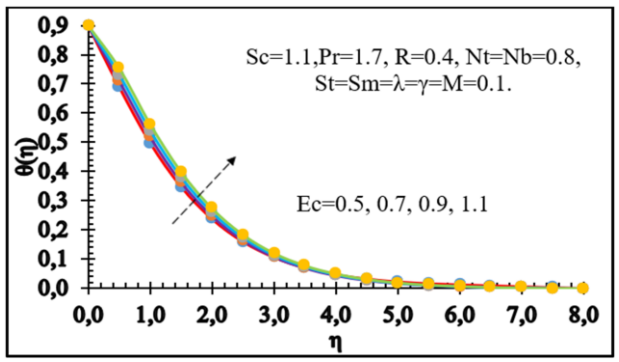

Fig. 7. Variation in $\theta(\eta)$ with Ec.

The Eckert number represents the conversion of kinetic energy into internal energy as the fluid works against viscous stresses, leading to heat generation within the system. This process, known as viscous dissipation, contributes to increasing the fluid temperature, particularly in high-speed or high-shear flows. As a result, the thickness of the thermal boundary layer increases, allowing heat to spread more effectively within the fluid. The presence of viscous dissipation plays a significant role in determining the temperature distribution, making it a crucial factor in high-speed flows, lubrication systems and thermal energy management.

Figure 8 exhibits the consequences of changing Sc. The Schmidt number (Sc) significantly affects the concentration profile by influencing the mass diffusion rate in the fluid.

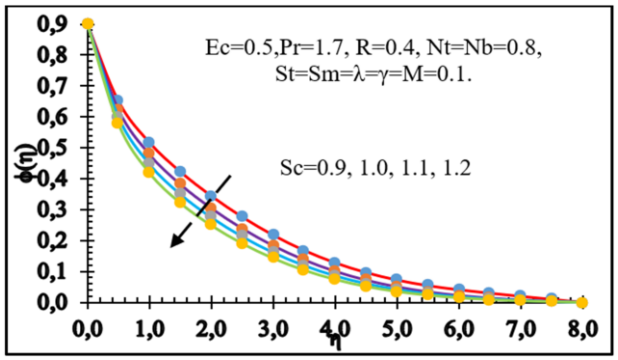

Fig. 8. Variation in $\phi(\eta)$ with Sc.

A higher Sc indicates lower mass diffusivity, meaning that particles diffuse more slowly, leading to a steeper concentration gradient and a thinner concentration boundary layer. Conversely, a lower Sc corresponds to higher diffusivity, allowing particles to spread more quickly and resulting in a more uniform concentration distribution. This effect is particularly important in applications such as chemical mixing, pollutant dispersion and mass transfer processes, where controlling the diffusion rate is essential for efficiency and effectiveness of the processes.

Figure 9 illustrates the effect of the solutal stratification parameter (S_m) on the concentration profile.

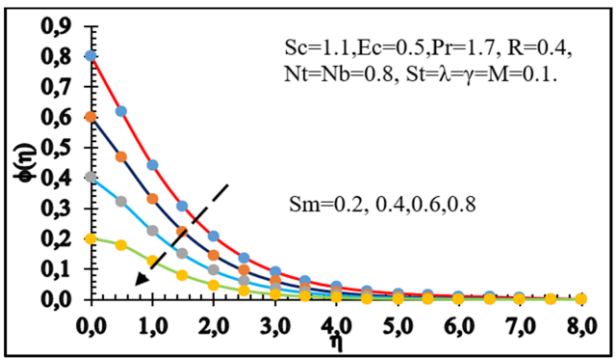

Fig. 9. Variation in $\phi(\eta)$ with S_m.

This parameter influences the concentration profile by affecting the mass transfer resistance within the fluid. As the stratification parameter increases, the difference in solute concentration between various layers of fluid becomes more pronounced, which restricts mass diffusion. This leads to a decrease in the overall concentration and the formation of a thinner solutal boundary layer. Increased stratification stabilises the concentration gradient, which is essential for ocean mixing, pollutant dispersion and chemical processing applications, where the controlled solute distribution is essential.

Figure 10 illustrates the influence of the chemical reaction parameter (γ) on the concentration profile $\phi(\eta)$. It is observed that, as γ increases, the concentration $\phi(\eta)$ decreases due to the enhanced rate of chemical reactions. Physically, a higher γ indicates more intense chemical activity, leading to a faster conversion of reactants into products. This rapid consumption of reactants reduces the overall concentration, particularly in regions where reactions are most active, such as reaction fronts. Additionally, a larger γ limits mass diffusion, resulting in a thinner concentration boundary layer. This effect plays a crucial role in chemical and industrial processes where reaction rates significantly impact mass transfer and fluid behaviour.

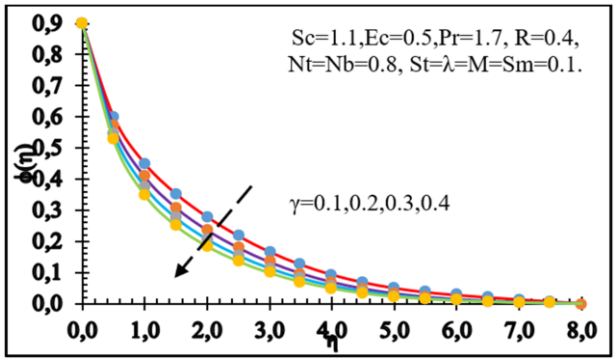

Fig. 10. Variation in $\phi(\eta)$ with γ.

Figure 11 presents the skin-friction coefficient as a function of the magnetic interaction parameter M for various values of the porosity parameter λ. An increase in M reduces the skin-friction coefficient, and a higher λ further decreases it.

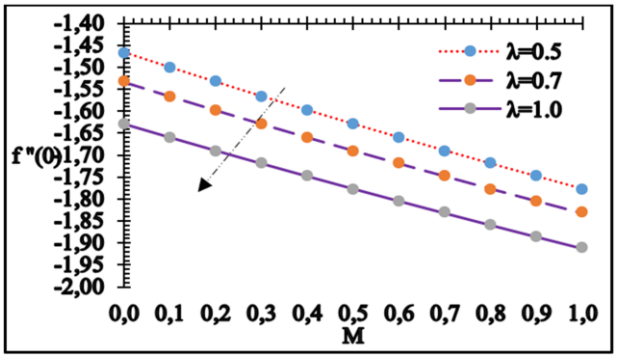

Fig. 11. Variation in skin friction with M and λ.

5. Conclusions

This research investigates, through numerical analysis, the effects of double stratification on nanofluid flow over an exponentially stretching surface. A two-dimensional, steady magnetohydrodynamic boundary layer flow of a thermo-solutally stratified nanofluid past an exponentially stretching sheet embedded in a porous medium is analysed. Using the shooting method, series-form solutions for the velocity, temperature and concentration profiles are derived. The numerical results are portrayed for several parameters. Similarity transformations and a strong numerical method – the shooting technique combined with the Adams–Moulton scheme were used to analyse the fluid behaviour.

Main results:

- An increase in the magnetic interaction parameter leads to a noticeable suppression of the velocity profile due to the enhanced Lorentz force opposing the flow.
- Elevated values of the thermal stratification parameter reduce the fluid temperature, while the solutal stratification parameter causes a decline in nanoparticle concentration, both effects attributed to the resistance against thermal and solutal diffusion.
- The thermal radiation parameter is found to negatively influence the Nusselt number, indicating reduced heat transfer efficiency in the presence of strong radiative effects.
- Heat transfer performance is enhanced with the increasing Schmidt number, Eckert number, thermophoresis parameter and Brownian motion parameter, reflecting enhanced energy transport due to mass diffusivity, viscous dissipation and nanoparticle dynamics.
- A rise in the chemical reaction parameter results in a lower nanoparticle volume fraction, which can be attributed to chemical dissipation processes occurring within the nanofluid.

References

[1] Choi, S.U.S. (1995). Enhancing thermal conductivity of fluids with nanoparticles. *ASME International Mechanical Engineering Congress and Exposition*, 66, 99–105. 12−17 November, San Francisco, USA.

[2] Buongiorno, J. (2005). Convective transport in nanofluids. *Journal of Heat Transfer*, 128, 240–250. doi: 10.1115/1.2150834

[3] Mushtaq, A., Mustafa, M., Hayat, T., & Alsaedi, A. (2016). Numerical study for rotating flow of nanofluids caused by an exponentially stretching sheet. *Advanced Powder Technology*, 27(5), 2223–2231. doi: 10.1016/j.apt.2016.08.007

[4] Shit, G., Haldar, R., & Mandal, S. (2017). Entropy generation on MHD flow and convective heat transfer in a porous medium of exponentially stretching surface saturated by nanofluids. *Advanced Powder Technology*, 28(6), 1519–1530. doi: 10.1016/j.apt.2017.03.023

[5] Reddy, P.S., & Chamkha, A.J. (2016). Soret and Dufour effects on MHD convective flow of Al_2O_3–water and TiO_2–water nanofluids past a stretching sheet in porous media with heat generation/absorption. *Advanced Powder Technology*, 27(4), 1207–1218. doi: 10.1016/j.apt.2016.04.005

[6] Gupta, S., Kumar, D., & Singh, J. (2018). MHD mixed convective stagnation point flow and heat transfer of an incompressible nanofluid over an inclined stretching sheet with chemical reaction and radiation. *International Journal of Heat and Mass Transfer*, 118, 378–387. doi: 10.1016/j.ijheatmasstransfer.2017.11.007

[7] Gireesha, B. J., Mahanthesh, B., Thammanna, G., & Sampathkumar, P. (2018). Hall effects on dusty nanofluid two-phase transient flow past a stretching sheet using KVL model. *Journal of Molecular Liquids*, 256, 139–147. doi: 10.1016/j.molliq.2018.01.186

[8] Magyari, E., & Keller, B. (1999). Heat and mass transfer in the boundary layers on an exponentially stretching continuous surface. *Journal of Physics D: Applied Physics*, 32(5), 577. doi: 10.1088/0022-3727/32/5/012

[9] Vajravelu, K. (2001). Viscous flow over a nonlinearly stretching sheet. *Applied Mathematics and Computation*, 124(3), 281–288. doi: 10.1016/S0096-3003(00)00062-X

[10] Cortell, R. (2007). Viscous flow and heat transfer over a nonlinearly stretching sheet. *Applied Mathematics and Computation*, 184(2), 864–873. doi: 10.1016/j.amc.2006.06.077

[11] Narender, G., Govardhan, K., & Sreedhar Sarma, G. (2020). Magnetohydrodynamic stagnation point on a Casson nanofluid flow over a radially stretching sheet. *Beilstein Journal of Nanotechnology*, 11, 1303–1315. doi: 10.3762/bjnano.11.114

[12] Narender, G., Govardhan, K., & Sreedhar Sarma, G. (2021). MHD Casson nanofluid past a stretching sheet with the effects of viscous dissipation, chemical reaction and heat source/sink. *Journal of Applied and Computational Mechanics*, **7**(4), 2040−2048. doi: 10.22055/jacm.2019.14804

[13] Murugesan, T., & Kumar, M.D. (2019). Viscous dissipation and Joule heating effects on MHD flow of a thermo-solutal stratified nanofluid over an exponentially stretching sheet with radiation and heat generation/absorption. *World Scientific News*, 129, 193−210.

[14] Hayat, T., & Nadeem, S. (2017). Heat transfer enhancement with Ag–CuO/water hybrid nanofluid. *Results in Physics*, 7, 2317−2324. doi: 10.1016/j.rinp.2017.06.034

[15] Hayat, T., Nadeem, S., & Khan, A.U. (2019). Numerical analysis of Ag–CuO/water rotating hybrid nanofluid with heat generation and absorption. *Canadian Journal of Physics*, 97, 644–650. doi: 10.1139/cjp-2018-0011

[16] Khan, S., & Sanjayanand, K. (2005). Viscoelastic boundary layer flow and heat transfer over an exponential stretching sheet. *International Journal of Heat and Mass Transfer*, 48, 1534–1542. doi: 10.1016/j.ijheatmasstransfer.2004.10.032

[17] Sajid, M., & Hayat, T. (2008). Influence of thermal radiation on the boundary layer flow due to an exponentially stretching sheet. *International Communications in Heat and Mass Transfer*, 35, 347–356. doi: 10.1016/j.icheatmasstransfer.2007.08.006

[18] Nadeem, S., Hayat, T., Malik, M.Y., & Rajputa, S.A. (2010). Thermal radiation effects on the flow by an exponentially stretching surface: A series solution. *Zeitschrift für Naturforschung A*, 65a, 495–503. doi: 10.1515/zna-2010-6-703

[19] Elbashbeshy, E.M.A. (2001). Heat transfer over an exponentially stretching continuous surface with suction. *Archives of Mechanics*, 53(6), 643–651.

[20] Swapna, D., Govardhan, K., & Narender, G. (2024). Magneto-micropolar nanofluid flow over a convectively heated sheet with nonlinear radiation, chemical reaction, and viscous dissipation. *Fusion Science and Technology*, 81(2), 132–143. doi: 10.1080/15361055.2024.2339700

[21] Reddy, S. S., Govardhan, K., & Narender, G. (2024). Numerical investigation of squeezing flow with mass and heat exchange between parallel plates: A study of velocity, temperature, and concentration distributions. *Radiation Effects and Defects in Solids*. doi: 10.1080/10420150.2024.2369127

[22] Thirupathi, G., Govardhan, K., & Narender, G. (2021). Radiative magnetohydrodynamics Casson nanofluid flow and heat and mass transfer past a nonlinear stretching surface. *Beilstein Archives Journal of Advanced Research in Numerical Heat Transfer*, 6(1), 1–21.

[23] Eid, M.R., & Nafe, M.A. (2020). Thermal conductivity variation and heat generation effects on magneto-hybrid nanofluid flow in a porous medium with slip condition. *Waves in Random and Complex Media*, 32(2), 1–25. doi: 10.1080/17455030.2020.1810365

[24] Narender, G., Govardhan, K., & Sreedhar Sarma, G. (2021). MHD Casson nanofluid past a stretching sheet with the effects of viscous dissipation, chemical reaction and heat source/sink. *Journal of Applied and Computational Mechanics*, 7(4), 2040–2048. doi: 10.22055/jacm.2019.14804

[25] Aly, E.H., & Pop, I. (2020). MHD flow and heat transfer near stagnation point over a stretching/shrinking surface with partial slip and viscous dissipation: Hybrid nanofluid versus nanofluid. *Powder Technology*, 367, 192–205. doi: 10.1016/j.powtec.2020.03.030

[26] Mathews, J., & Hymavathi, T. (2024). Unsteady magnetohydrodynamic free convection and heat transfer flow of Al_2O_3–Cu/water nanofluid over a non-linear stretching sheet in a porous medium. *Archives of Thermodynamics*, 45(1), 165–173. doi: 10.24425/ather.2024.150449

[27] Hayat, T., Rashid, M., & Imtiaz, M. (2017). MHD effects on a thermo-solutal stratified nanofluid flow on an exponentially radiating stretching sheet. *Journal of Applied Mechanics and Technical Physics*, 58, 214–223. doi: 10.1134/S0021894417020043